SO_2 DATA FROM THE OZONE MONITORING INSTRUMENT

N.A. Krotkov[(1)], K. Yang [(1)] , A. Krueger[(2)], S.A. Carn[(2)], P.K. Bhartia[(3)], P.F. Levelt[(4)]

[(1)] GEST/UMBC, Baltimore, MD (USA), Email: Krotkov@mhatter.gsfc.nasa.gov
[(2)] JCET/UMBC, Baltimore, MD (USA), Email: akrueger@umbc.edu
[(3)] NASA/GSFC, Greenbet, MD (USA), Email: Pawan.Bhartia@nasa.gov
[(4)] KNMI, DeBuilt (Netherlands), Email: Pieternel.Levelt@knmi.nl

ABSTRACT

We discuss collection 2 SO_2 data from the Dutch-Finnish Ozone Monitoring Instrument (OMI) on board NASA EOS/Aura spacecraft and show examples of detected volcanic and anthropogenic SO_2 emissions. Quantification of anthropogenic SO_2 emissions requires collection 3 reprocessing available in the fall 2007.

1. INTRODUCTION

Sulfur Dioxide (SO_2) is a short-lived gas primarily produced by volcanoes, power plants, refineries, metal smelting and burning of fossil fuels. Where SO_2 remains near the Earth's surface, it is toxic, causes acid rain, and degrades air quality. SO_2 that moves into the free troposphere forms aerosols that can alter cloud reflectivity and precipitation. In the stratosphere, volcanic SO_2 forms long-lived sulfate aerosols that can result in climate change. The first quantitative data on the mass of SO_2 in a major eruption (El Chichon, 1982) was obtained from the six-UV band NASA Nimbus-7 Total Ozone Mapping Spectrometer (TOMS) [1]. All significant eruptions since 1978 have now been measured by the series of TOMS instruments (Figure 1) [1-4]. The SO_2 detection sensitivity was limited to large volcanic clouds by the discrete TOMS wavelengths that were designed for total ozone measurements [1,4]. Greatly improved sensitivity was demonstrated through detection of volcanic and anthropogenic SO_2 in Global Ozone Monitoring Experiment (GOME) [5,6] and Scanning Imaging Spectrometer for Atmospheric Cartography (SCIAMACHY) [7] full spectrum UV data. However, these sensors need several days to acquire a contiguous global map and hence could miss short-lived pollution events. The NASA EOS Aura platform [8], launched on July 15, 2004, carries the Ozone Monitoring Instrument (OMI), a hyperspectral UV/Visible spectrometer with a 2600 km swath for daily, global contiguous mapping that was provided by the Netherlands Agency for Aerospace Programs (NIVR) in collaboration with the Finnish Meteorological Institute (FMI) to the NASA EOS Aura mission for continued monitoring of ozone and other trace gases [9]. KNMI (Royal Netherlands Meteorological Institute) is the Principal Investigator institute. Reflected sunlight in a fan-shaped narrow field of view is dispersed by a spectrometer and imaged in spatial –spectral dimensions on two-dimensional Charge Coupled Device (CCD) detectors, one for UV and one for visible bands [10]. OMI SO2 algorithm uses data from the 310–365 nm UV-2 band with spectral resolution of ~0.45 nm [10]. Data are collected from the pushbroom swath in 2-sec intervals corresponding to 13 km along-track resolution. Pixels are binned in 60 cross-track positions to provide a nadir resolution of 24 km. The OMI Level-2 SO2 Product, 'OMSO2,' is publicly available from the NASA's GSFC Earth Sciences (GES) Data and Information Services Center (DISC) at http://disc.gsfc.nasa.gov/Aura/OMI/omso2.shtml and examples and documentation at http://so2.umbc.edu/omi

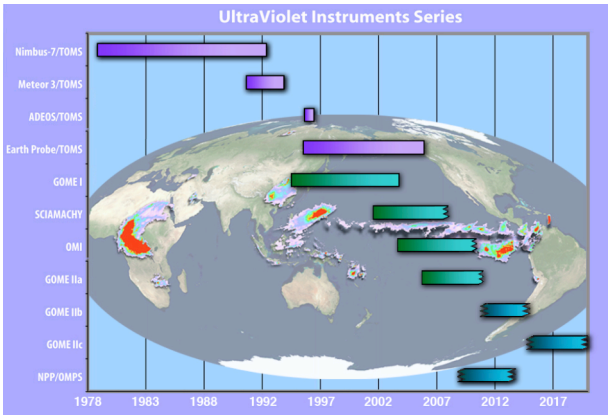

Figure 1. Timeline of past (purple), present (green), and planned (blue) mapping UV instrument datasets available for a 40+ year record of SO_2 emissions, superimposed on a global map of sulfur dioxide clouds detected with OMI in 2005/2006. US instruments include TOMS on Nimbus-7 (1978-1993), Meteor-3 (1991-1994), ADEOS (1996-1997) and Earth Probe (1996-2005) (http://toms.umbc.edu),and the future OMPS on NPOESS Preparatory Project (NPP, http://jointmission.gsfc.nasa.gov/), to be followed by operational flights on NPOESS satellites. European instruments include GOME flying on ESA's ERS-2 satellite since July 1995 [5], OMI on EOS Aura (2004 – current) [9,10], SCIAMACHY operated from ESA's ENVISAT satellite since August 2002 [7] and GOME-2 flying on a series of EUMETSAT MetOp satellites since October 2006.

2. ALGORITHM

In the OMSO2 product the three reported total SO_2 values correspond to the SO_2 in the Planetary Boundary Layer (PBL, below 2 km) from anthropogenic sources, SO_2 distributed between 5 and 10 km emitted by passive volcanic degassing in the free troposphere, and SO_2 distributed between 15 and 20 km representing injection from explosive volcanic eruptions. All PBL data are processed with the Band Residual Difference (BRD) algorithm [11], while all 5 km and 15 km data are processed with the Linear Fit (LF) algorithm [12]. Both algorithms use the OMI TOMS –like total ozone retrieval, 'OMTO3' [13] as a linearization step to derive initial estimate of total ozone (assuming zero SO_2) and the wavelength independent Lambertian effective surface reflectivity (LER). The OMTO3 algorithm accomplishes this by matching the calculated radiances to the measured radiances at a pair of wavelengths (317.5 nm and 331.2 nm under most conditions). The residuals at the 10 other wavelengths (Figure 2) are then calculated as the difference between the measured and the computed N-values ($N=-100*log_{10}(I/F)$, I is Earth radiance and F is solar irradiance) that account for the effects of multiple Rayleigh scattering, ozone absorption, Ring effect, and surface reflectivity. In the presence of SO_2, the residuals contain wavelength structures that correlate with the SO_2 absorption cross sections [11]. The residuals also have contributions from other error sources. To reduce this interference, the empirical correction to the residuals is performed before retrieval of the final state is attempted [12]. Both the BRD and LF algorithms use the corrected residuals as their inputs to derive SO_2 column amount. The BRD uses differential residuals at the three most SO_2 sensitive pairs [11], while the LF minimizes different

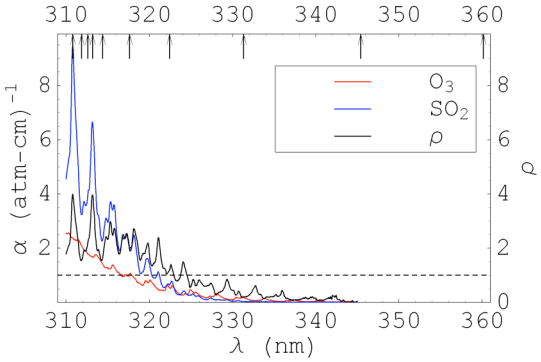

Figure 2. Absorption coefficients of SO_2 and O_3 and their ratio as a function of wavelength. The arrows indicate the central wavelengths used in the algorithm.

subsets of residuals by simultaneously adjusting SO_2, ozone and quadratic polynomial coefficients of the LER spectral dependence. The subsets are determined by the process of dropping the shortest wavelength bands one at a time until the 322nm band is reached. The largest SO_2 retrieval is reported as the final estimate. Figure 3 compares SO_2 retrievals from LF (5km) and BRD (AMF for 5km) algorithms for OMI observation (on October 23, 2005) of the Sierra Negra volcanic plume. Both algorithms show the same spatial extent but very different dynamic range in the total SO_2 distributions. The LF retrieval produces much higher SO_2 concentrations near the vent of the volcano, and the concentrations drop off quickly as this plume is dispersing. The BRD image is quite similar to that of the LF, particularly in the area with low LF SO_2 concentrations, but the obvious difference is the complete lack of high SO_2 concentrations in the BRD image. Therefore, all operational volcanic data (5km and 15km) are processed with the LF algorithm [12].

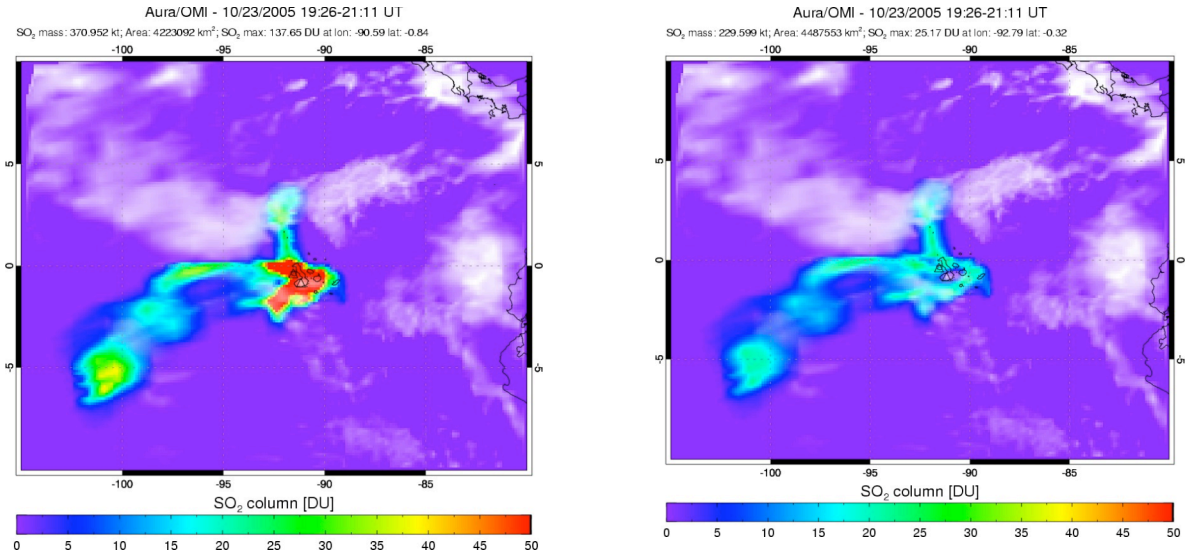

Figure 3. OMI observations of the volcanic plume on 23 October 2005, emitted from Sierra Negra Volcano (summit elevation of 1124 km) in the Galapagos Islands. (Left) 5 KM retrievals from LF algorithm [11]. (Right) 5 KM retrievals from BRD algorithm [12]. White regions are meteorological clouds (OMI reflectivity [13]).

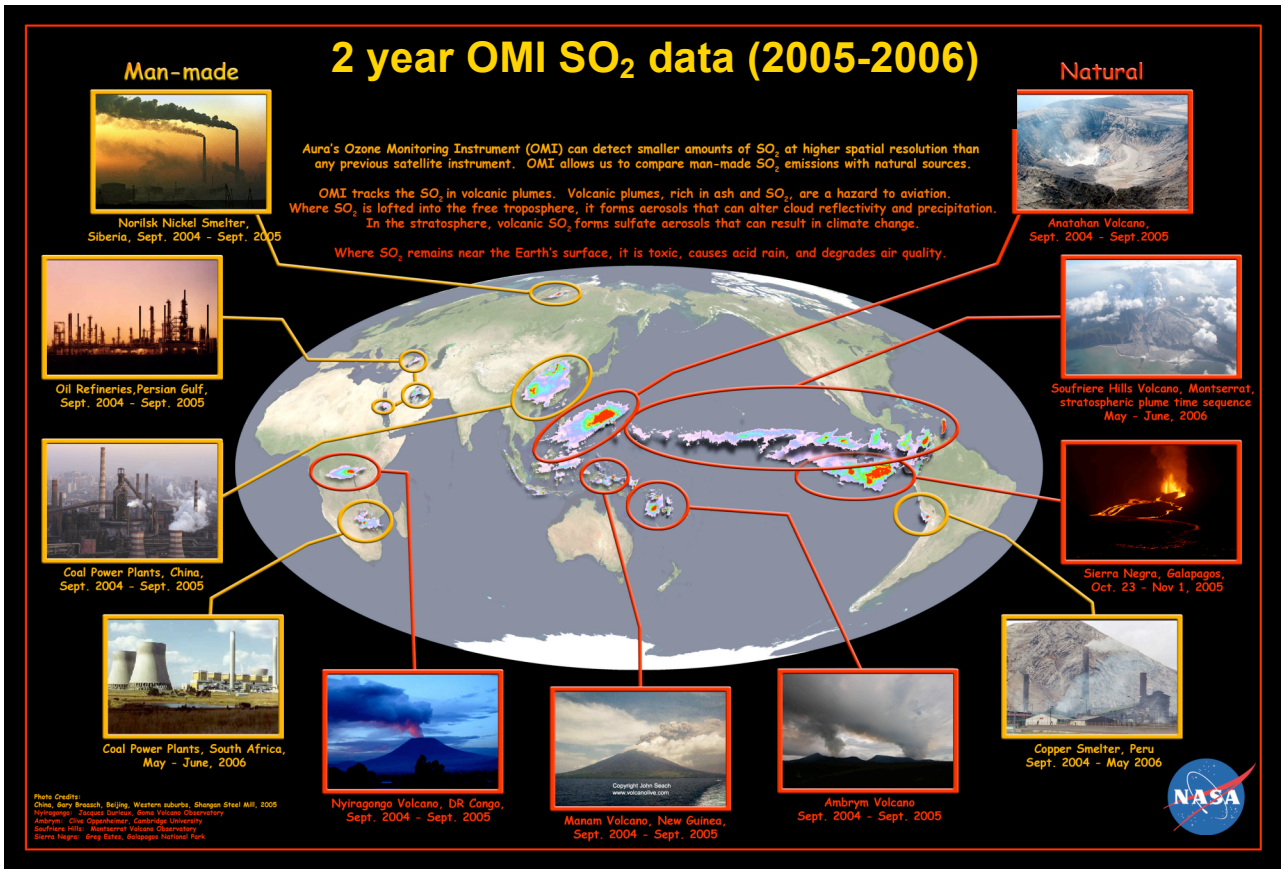

Figure 4. Two-year overview of OMI SO_2 data (2005-2006).

3. OMI SO_2 DATA OVERVIEW

Assessment of OMI data quality is difficult as minimal SO_2 validation data are currently available. Errors will not necessarily be randomly distributed over the globe, but will typically increase with solar zenith angle, large ozone or SO_2 column amounts and in the presence of clouds and heavy aerosol loading.

3.1 Volcanic SO_2 emissions

The OMI SO_2 volcanic data set continues he TOMS SO_2 record, which covers a quarter-century [1-4] (http://toms.umbc.edu), but the improved sensitivity and smaller footprint of OMI will extend the range of detection to smaller eruptions and older clouds, and to degassing volcanoes. The LF algorithm provides good retrievals for small to moderate SO_2 loading (up to ~30 DU), but underestimates the true SO_2 amount for higher loadings [12]. The noise in background areas is less than 0.3 DU (1standard deviation) and bias <0.4DU at low and mid-latitudes. Both the bias and noise increase for solar zenith angles greater than 70° and in the region of South Atlantic Anomaly.

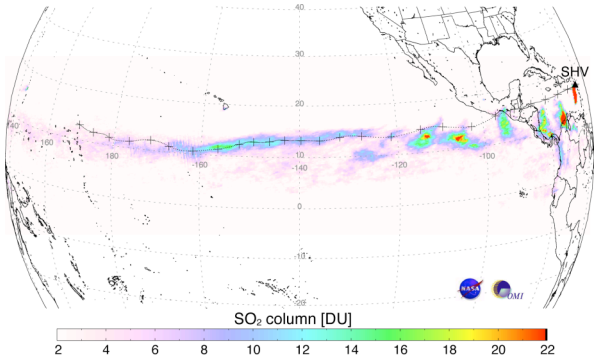

Figure 5. Cumulative SO_2 measured by OMI in the Soufriere Hills volcano (SHV Montserrat, Lesser Antilles) volcanic cloud from 20 May - 6 June 2006 as the cloud crossed the Pacific Ocean. The dotted line is a HYSPLIT forward trajectory for a cloud at 20 km altitude, initialized at 11UT on 20 May at SHV, with crosses plotted every 12 hours. The trajectory covers 315 hours (~13 days) of cloud transport [14].

Visualization of daily OMI SO2 data allowed rapid appraisal of the most significant volcanic SO_2 emitters, which in 2006 included Merapi (Indonesia), Tungurahua (Ecuador), Soufriere Hills (Montserrat), Aoba (Vanuatu), Nyiragongo (DR Congo) and Ubinas (Peru). These measurements highlight the deficiencies of previous compilations of volcanic SO_2 emissions, which were biased towards accessible, frequently monitored volcanoes. The eruption of Soufriere Hills volcano (Montserrat) on May 20, 2006 resulted in a stratospheric injection of ~0.2 Tg of SO_2 [14]. Despite the modest size of the SO_2 cloud (2 orders of magnitude lower in mass than Pinatubo [3]), OMI was able to track it for over 3 weeks and ~16,000 miles as it traveled westwards from the volcano (Figure 5). The Soufriere Hills eruption and one of similar magnitude at Rabaul (Papua New Guinea) in October 2006 were the largest volcanic SO_2 injections of 2006.

3.2 Anthropogenic SO2 pollution

Heavy anthropogenic emissions were detected on a daily basis. For example, emissions from two Peruvian smelters (La Oroya and Ilo) were detected in up to 80% of OMI overpasses (Figure 6). SO_2 production by each smelter in this period was quantified and compared with contemporaneous emissions from active volcanoes in Ecuador and Colombia [15].

A first OMI SO2 validation study was conducted using aircraft in-situ SO_2 data collected over Shenyang in NE China as part of EAST-AIRE field campaign in April 2005 [16, 17]. Between April 5 and April 7 a cold front traveled across continental China on to the Sea of Japan

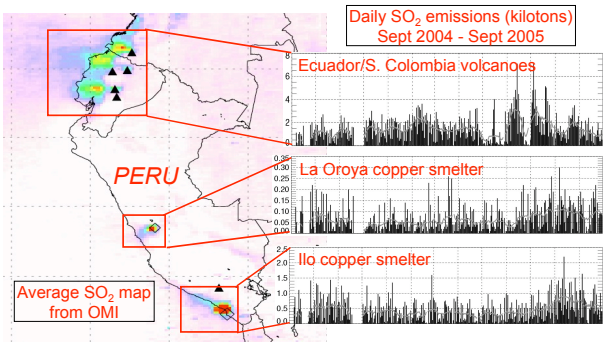

Figure 6. Left: Average OMI SO2 vertical column over southern Colombia, Ecuador and Peru, Sep 2004 – June 2005. Image is scaled from low (white) to high (red) values of average SO2 vertical column amount. Weak SO2 plume continuing off Ecuador is due to higher altitude, longer lifetime and greater dispersion of the volcanic S emissions. Average concentrations are higher close to the smelters due to lower dispersion of these boundary layer emissions.(Right): Daily SO2 burdens for 3 main source regions measured by OMI. Note that the vertical scale varies on the SO2 burden plots [15].

[16]. The OMI measurements of SO2 agree with the aircraft in situ observations of high concentrations of SO2 (ca ~2 DU) ahead of the cold front and lower concentrations behind it (Figure 7 [17]). This comparison demonstrates that OMI can distinguish between background SO2 conditions and heavy

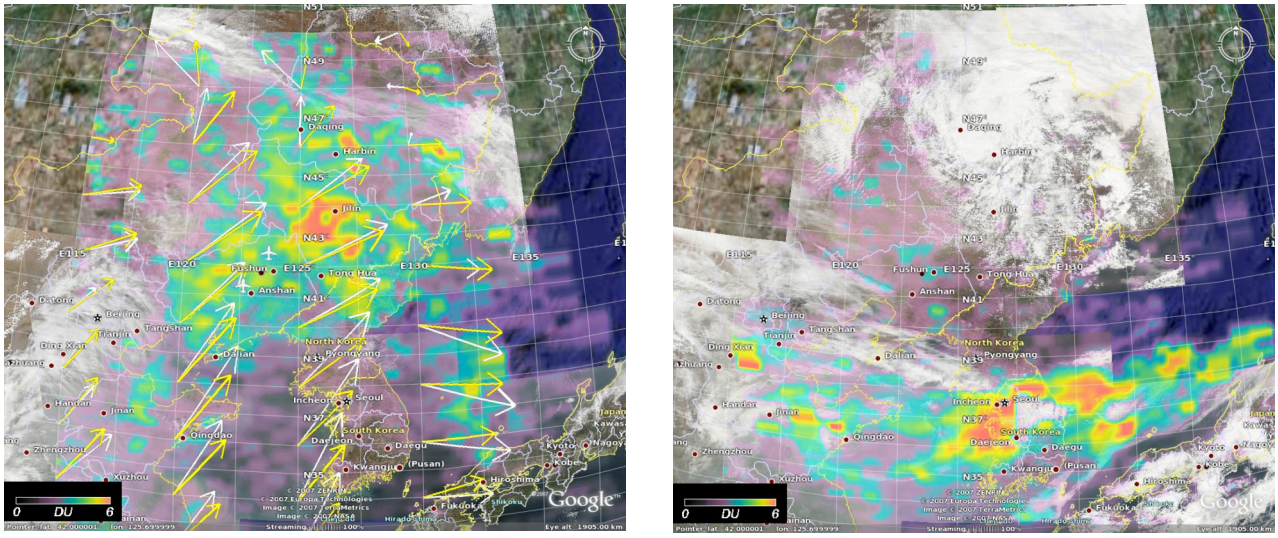

Figure 7. OMI SO_2 (color) and AQUA/MODIS RGB composites during East-AIRE aircraft campaign (flight region is shown with aircraft symbols) ahead of cold front on April 5 (left) and behind cold front on April 7 (right) 2005. Arrows show NCEP winds at surface and 800hpa. Apparent high SO2 concentrations (~5DU) provide evidence of SO2 plume lofting above the PBL and/or underlying clouds. Both effects increase OMI sensitivity, so the operational PBL SO2 data should be corrected for both effects [17].

pollutions on a daily basis. The regional plume of SO_2, detected on 5 April over Shenyang area, was tracked for 4 days by OMI providing evidence for pollution lofting from the PBL and a large-scale impact of Chinese pollutant emissions.

The noise in OMI PBL data (with operational air mass factor, AMF of 0.36) is 1 to 1.5DU and almost independent on the region or season. Therefore, spatial averaging of OMI data reduces the noise as square root of the number of individual Field-of-view (IFOV) data averaged.

Comparisons with aircraft allowed quantifying the OMI bias (up to 2.5DU, OMI being higher). Averaging OMI data over flight region (2^ox2^o) reduces the biases to ~1DU. The smallest bias ~0.4DU was detected on the clean day over China, while zero bias was determined over pristine ocean region [17]. Both noise and bias are affected by OMI radiance/irradiance calibration. A preliminary comparison with collection 3 test data has shown that improved stray light correction substantially reduces positive OMI bias on polluted days over EAST-AIRE region. Therefore, we recommend using collection 3 reprocessed data that will be available in the fall 2007

For quantifying anthropogenic SO_2 emissions the operational AMF should be corrected to account for effects of observational geometry, total ozone, surface reflectivity, SO_2 vertical distribution, aerosols and clouds. AMF corrections can be performed off-line using AMF regressions parameterizations [17]. The corrections for absorbing aerosols over China (typical single scattering albedo ~0.9) using OMI industrial aerosol model [18] resulted in almost unchanged bias. However, dust and organic carbon aerosols (absorption increases at short UV wavelengths) would have much larger effect. Therefore quantifying spectral dependence of aerosol absorption at SO2 wavelengths (310nm-330nm) is critical for the accurate estimate of the SO2 mass using satellite UV measurements.

Using weekly, monthly or annual average SO_2 maps even weaker degassing and pollution stationary sources can be detected. SO_2 emissions have been measured by OMI over known sources of air pollution, such as the Ohio valley in the USA, eastern China, and Eastern Europe (e.g., Fig.8). We note that the SO_2 enhancements detected by OMI from sources in S. E. Europe (chiefly in Romania and Bulgaria (Fig. 8, middle)) correspond in both location and approximate column amount to GOME observations from February 1998 reported in [6]. These SO_2 emissions are sourced from lignite-burning power plants in the Balkan region [6].

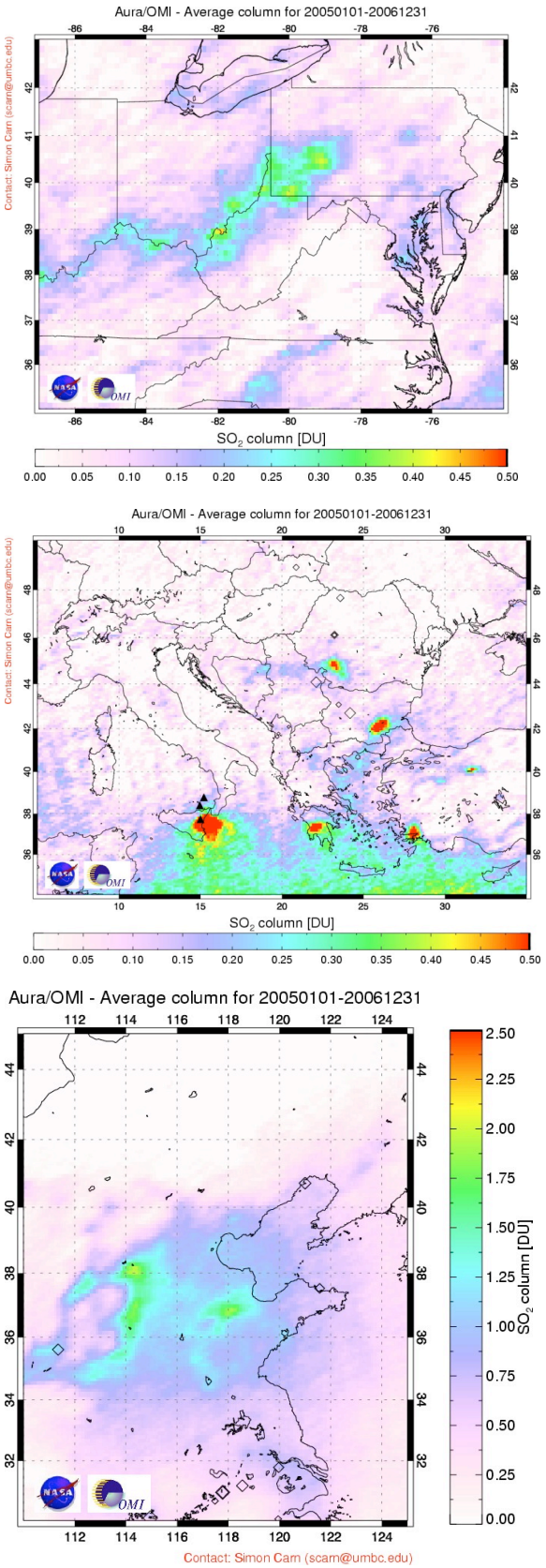

Figure 8. 2 year average SO_2 burdens over Ohio valley (US, top), SE Europe (middle) and China (bottom).

4. CONCLUSION

Using OMI data, users can directly compare daily global SO_2 emissions from anthropogenic and volcanic sources for the first time, and thus provide important new constraints on the relative magnitude of these fluxes. Such measurements are essential given the growing concern over the effects of anthropogenically-forced climate change and intercontinental transport of air pollution. The fast operational OMI SO_2 retrieval is also amenable to operational SO_2 alarm development, and near real-time application for aviation hazards and volcanic eruption warnings.

The operational (version 1) algorithm sensitivity does not represent the maximum sensitivity theoretically achievable with OMI, and hence future algorithm improvements (i.e. spectral fitting) as well as improvements in instrument calibrations (i.e collection 3 data) should allow even weaker SO_2 sources to be monitored routinely. These measurements are expected to produce the best estimates to date of the volcanic contribution to global atmospheric SO_2 abundances.

5. REFERENCES

1. Krueger, A. J. (1983). Sighting of El Chichon sulfur dioxide clouds with the Nimbus 7 Total Ozone Mapping Spectrometer", *Science* **220**, 1277-1379.
2. Bluth, S.D. Dorion, C.C. Schnetzler, A.J. Krueger, and L.S. Walter. (1993). The contribution of explosive volcanism to global atmospheric sulfur dioxide concentrations", *Nature* **366**, 327-329.
3. Krueger, A.J., Schaefer, S. J., Krotkov, N.A., Bluth, G. & Barker, S. (2000). Ultraviolet remote sensing of volcanic emissions, in *Remote Sensing of Active Volcanism*, *Geophys. Monogr. Ser.*, **116**, AGU, ed. by P. J. Mouginis-Mark, J. A. Crisp, and J. H. Fink, 25-43.
4. Carn, S.A., Krueger, A.J., Bluth, G., Schaefer, S. Krotkov, N., Watson, I. & Datta, S. (2003). Volcanic eruption detection by the Total Ozone Mapping Spectrometer (TOMS) instruments: a 22-year record of sulphur dioxide and ash emissions, in *Volcanic Degassing*, *Spec. Publ. Geol. Soc. Lon.* **213**, ed. by C. Oppenheimer, D. M. Pyle, and J. Barclay, 177-202.
5. Burrows, J.P., M. Weber, M. Buchwitz, V. Rozanov, A. Ladstätter-Weissenmayer, A. Richter, R. de Beek, R. Hoogen, K. Bramstedt, K.-U. Eichmann, M. Eisinger, and D. Perner, (1999). The Global Ozone Monitoring Experiment (GOME): Mission concept and first scientific results", *J. Atm. Sci.*, **56** 151-175.
6. Eisinger, M. & J. P. Burrows, (1998). Tropospheric Sulfur Dioxide observed by the ERS-2 GOME instrument, *Geophys. Res. Lett*, **25,** 4177-4180, 1998.
7. Bovensmann, H. et al., (1999). SCIAMACHY – Mission objectives and measurement modes, *J. Atmos. Sci.*, 56, 127-150.
8. Schoeberl, M.R., Overview of the EOS Aura mission. (2006). *IEEE Trans. Geo. Rem. Sens*, **44**(5), 1066-1074.
9. Levelt, P.F., Oord, van den,G. H. J., Dobber, M.R. A. Malkki, H. Visser, J. de Vries, P. Stammes, J. Lundell, H. Saari, (2006). The Ozone Monitoring Instrument. *IEEE Trans. Geo. Rem. Sens.* **44**(5), 1093-1101.
10. Dobber, M. R., et al., (2006). Ozone Monitoring Instrument description, performance and calibration", *IEEE Trans. Geo. Rem. Sens.* **44**(5), 1209-1238.
11. Krotkov, N., A., S. A. Carn, A.J. Krueger, P.K. Bhartia, and K. Yang (2006), Band residual difference algorithm for retrieval of SO2 from the AURA Ozone Monitoring Instrument (OMI), in print, *IEEE Trans. Geo. Rem. Sens.* **44**(5), 1259-1268.
12. Yang, K., N.A. Krotkov, A.J.Krueger, S.A. Carn, P.K. Bhartia, P.F. Levelt. (2007) Retrieval of large volcanic SO2 columns from the AURA OMI: comparison and limitations, under review, *J. Geophys. Res., AURA validation special issue*.
13. Bhartia,P.K. C. W. Wellemeyer, "TOMS-V8 total ozone algorithm" *In OMI Algorithm Theoretical Basis Document, OMI Ozone Products, vol. 2* , version 2, Ed by P. K. Bhartia, NASA/Goddard Space Flight Center, 2002. Available: http://eospso.gsfc.nasa.gov/eos_homepage/for_scientists/atbd/docs/OMI/ATBD-OMI-02.pdf
14. Carn, S.A., N.A. Krotkov, K. Yang, R.M. Hoff, A.J. Prata, A.J. Krueger, S.C. Loughlin, P.F. Levelt, Extended observations of volcanic SO2 and sulfate aerosol in the stratosphere, Atmos. Chem. Phys. Discussions, 2007a
15. Carn, S.A., N.A. Krotkov, A.J. Krueger, K. Yang, P.F. Levelt, (2007b) Sulfur dioxide emissions from Peruvian copper smelters detected by the Ozone Monitoring Instrument", Geophys. Res. Lett.
16. Dickerson, R. et al. (2007) Aircraft observations of dust and pollutants over NE China: Insight into the meteorological mechanisms of long-range transport, *J. Geophys. Res., EAST-AIRE special issue*, under review.
17. Krotkov, N. A., et al. (2007) OMI SO2 validation over NE China, *J. Geophys. Res, Aura validation special issue*, under review
18. Torres, O., A. Tanskanen, et al., (2007) Aerosols and surface UV products from OMI observations: An overview, J. Geophys. Res., *J. Geophys. Res, Aura validation special issue*, under review